Chapter 15
Ultrafast Optical Techniques for Communication Networks and Signal Processing

Bhavin J. Shastri, John Chang, Alexander N. Tait, Matthew P. Chang, Ben Wu, Mitchell A. Nahmias and Paul R. Prucnal

Abstract Wireless communications, for data services in particular, have witnessed an exponential growth, and wireless spectrum shortages necessitate increasingly sophisticated methods to use spectrum efficiently. The backhaul of nearly all wireless data networks is fiber-optic. Analog optical signal processing techniques, or microwave photonics, provides an ideal platform for processing wireless information before it is transported to data aggregation centers by fibers. It is in this context that we present recent advances in optical signal processing techniques for wireless radio frequency (RF) signals. Specifically, this chapter is devoted to the discussion of photonic architectures for wideband analog signal processing, including RF beamforming, co-channel interference cancellation, and physical layer security. Photonics offers the advantages not only of broadband operation, but reduced size, weight, and power, in addition to low transmission loss, rapid reconfigurability, and immunity to electromagnetic interference.

15.1 Introduction

The use of wireless communication is growing exponentially. In June 2012, more than 5.6 billion subscribers had access to and were using a wireless device, nearly 80 % of the total world population of 7.02 billion [1]. By the end of 2017, more than 90 % of the world's population is expected to have access to mobile broadband 3G devices. This statistic demonstrates the importance of mobile wireless com-

B.J. Shastri and J. Chang—equal contribution.

B.J. Shastri · J. Chang · A.N. Tait · M.P. Chang · B. Wu · M.A. Nahmias · P.R. Prucnal (✉)
Princeton University, Princeton, NJ 08544, USA
e-mail: prucnal@princeton.edu

S. Wabnitz and B.J. Eggleton (eds.), *All-Optical Signal Processing*,
Springer Series in Optical Sciences 194, DOI 10.1007/978-3-319-14992-9_15

munication in the current decade and beyond. By the end of 2015, mobile traffic is expected to double. Nearly 11 exabytes will be transmitted *per month* in 2016, more than four times the quantity transmitted in the last 2 years. Mobile broadband, growing with a compound rate of 80 %, is shaping to become one of the most successful and fastest growing industries in history. This growth in the mobile market has been spurred by two key factors: fast, powerful, and ubiquitous mobile networking, and high-performance smartphones with a million-plus mobile applications [2]. The rapid shift from traditional headsets to smartphones has been attributed to increased performance and lower energy consumption.

As wireless communication continues to grow, the radio frequency spectrum will become increasingly scarce. The climb in the demand for smartphones and faster, large-coverage next-generation mobile networks will be paralleled by a demand for available bandwidth—but this demand comes with an equal increase in wireless spectrum use. There will be two technological barriers that will result from these increased demands: first, wireless spectrum is finitely limited and is constrained, and spectral efficiency use must be carefully managed as bandwidth begins to grow. Second, a heavily saturated spectrum means interference from neighboring devices and frequency bands could negatively impact data rates and signal bandwidth.

One way of addressing both these escalating problems is through the use of interference cancellation. Although noise-filtering and other post-processing methods could reduce interference, a more effective technique would involve cancelling interference directly in the radio frequency (RF) domain. This technique reduces interference and increases bandwidth availability. As a result, the application of RF interference cancellation could have a significant impact on the alleviation of overcrowding in the wireless domain.

Figure 15.1 shows a typical scenario seen by a wireless communication system (such as a radar, for instance). There is a clear target, whose information we wish to receive. Along with that information, however, is environmental clutter and other interfering signals. Clutter results from the local environment, which can be exacerbated by complex terrain or weather conditions. Noise and signals from other sources also contribute to interference. Our goal is to design a system to extract a target signal, or signal of interest (SOI), from this noise.

Adaptive arrays in electronics (Fig. 15.2) have been used to increase signal-to-noise ratio (SNR) in the presence of dynamic interference and noise in wireless communication systems since the 1960s and are a perfect solution for the problem outlined above [3]. Arrays, instead of singular antennas, give the advantages of higher gain (through multiple antennas), electronic beam forming (steering of the beam-pattern without physical movement), and adaptive cancellation (by taking advantage of beamforming capabilities). Because these adaptive arrays are both tunable and easily reconfigurable, they are more reliable than conventional antennas and can be used in multiple scenarios across different fields. However, electronic systems suffer from two major deficits: beam squinting and limited bandwidth. Beam squinting arises from the use of phase shifters, which degrades an antenna array's beam-pattern with frequency, resulting in different responses for signals of

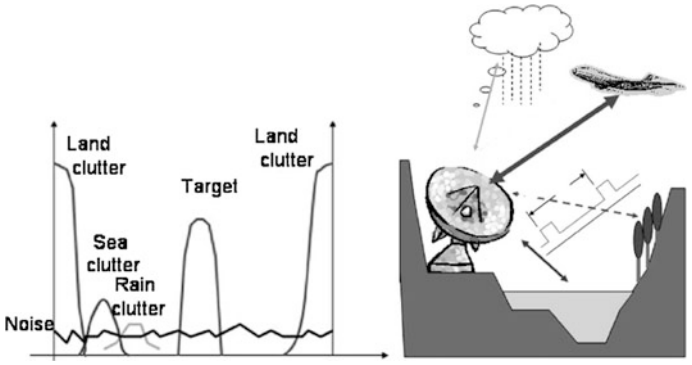

Fig. 15.1 Typical clutter in wireless environment [5]

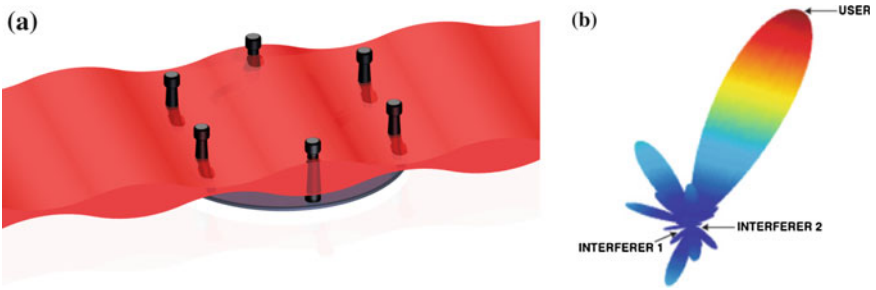

Fig. 15.2 **a** An antenna array uses phase information to detect the direction of arrival of an incident wave. **b** Adaptive array coverage: a representative depiction of a main lobe extending toward a user with null directed toward two co-channel interferers [3]

different frequencies. Bandwidth limitations result from the limited speed of electronic devices. This limits the use of electronic systems to narrow-band signals. Furthermore, losses increase for electronic systems past 100 MHz, limiting systems that wish to operate in the tens of GHz.

While wireless networks have seen a rapid increase their bandwidth capabilities, optical networks have been popular for a decade and their capabilities greatly overshadow even the fastest wireless standard. Figure 15.3 compares wireless and optical networks. Optical network growth follows that of wireless networks and is at least 10× faster at each step. Because of the inherent bandwidth superiority of optics, wireless data is always aggregated and backhauled to data centers by the way of optical networks. This serves as the perfect backdrop for an optical cancellation system sandwiched in-between the wireless base stations and the optical backhaul network. Wireless signals are modulated onto the optical domain and then directly processed using a photonic cancellation system before being sent over an optical network. This field is known as microwave photonics, which is an interdisciplinary area that studies the interaction between microwave and optical signals [4].

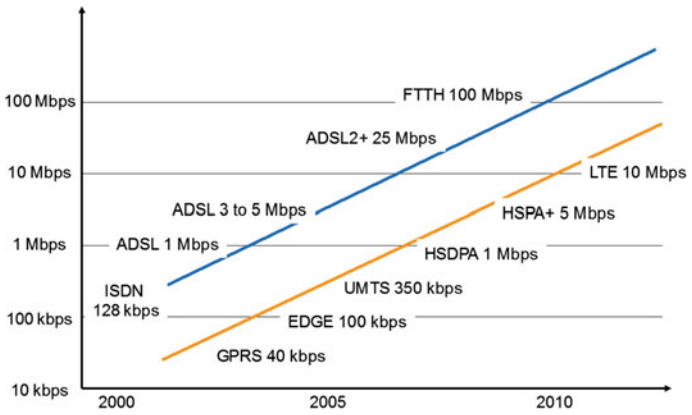

Fig. 15.3 Advances in wireless and optical capacity [1]

Optical systems bring advantages inherent to the physics of photonics, which include low loss, high bandwidth, immunity to electromagnetic interference (EMI), tunability, and reconfigurability [5]. Most importantly, optical systems solve both the beam squinting and bandwidth limitations of electronic systems. By using optical delay lines, true-time delay (TTD) antenna arrays eliminate beam squinting [4]. Electronic systems oftentimes use multiple pieces of equipment to cover a wide bandwidth. In contrast, because photonic systems keep the signal in the optical domain, they can utilize the tremendous bandwidth of optics (up to THz) to process fast-varying RF signals without degrading bandwidth using a single set of optical equipment. This gives optical systems savings in size, weight, and power (SWAP), especially for situations where compactness and light weight are important (i.e. aviation). Furthermore, optical interference cancellation in conjunction with optical backhaul networks makes it possible to centralize signal processing in one shared location. Centralization allows for equipment sharing, dynamic allocation of resources, simplified system operation and maintenance [5]. Different operators can share resources using the same optical backhaul network to minimize cost and energy.

Microwave photonics filters (MPFs) are an alternative photonic technology and have an enormous amount of bandwidth selectivity. They can be employed in optical systems for either channel rejection or channel selection to cancel interfering signals that are picked up by antennas [4, 6, 7]. Unique to photonics filters is the rejection of signals in the optical domain using optical signal processing techniques. MPFs can be tuned to cancel a selected frequency band across a large bandwidth from MHz to hundreds of GHz [5, 8].

This chapter investigates an optical method for wireless interference cancellation systems using *optical signal processing* techniques. We marry the field of adaptive arrays and microwave photonics. Beam-steering is done by adaptive antenna arrays with processing done all-optically by MPFs. By utilizing the broad bandwidth and

high capacity of optics to address growing problems in mobile communication market, we hope to create a photonic interference cancellation system with wide-ranging impact, both economically and scientifically.

15.1.1 Scenario of Interest

This chapter is interested in a scenario with dynamically changing noise and interference in the presence of a SOI. We assume that we have a receiver either in a dense urban environment, such as in a mobile phone setting, or a crowded indoor environment, such as in a WIFI network. We wish to follow a mobile transmitter as it is broadcasting the SOI, so that its location, and possibly frequency, is constantly changing. To make the problem even more challenging, we assume that we cannot know anything about the SOI, other than its frequency, and have no information of the content of this signal.

We make several additional assumptions: we must cancel an interfering signal to receive the SOI. The SOI is much smaller in power than the interference. We also lack knowledge of both the location and frequency of the interfering signal. The interference is both dynamic and spontaneous, with multiple interferers appearing and disappearing with shifting frequencies. We also do not know the relative power or direction between the SOI and the interferers.

Since we are in a crowded environment (either urban or indoors), we can assume high levels of dynamically changing noise. Transmitters and other users may appear or disappear spontaneously and change locations, which is in addition to the background noise that permeates throughout the wireless spectrum. Interference in the form of multipath fading will be detrimental to signal quality. In the indoor scenario, near-field signals dominate, with wavefronts that may not be planar or uniform with respect to the receiver.

The problem requires a two-part solution. First, filters for both space and frequency are required to rid the interference and noise from the SOI. Secondly, an adaptive method is needed to quickly keep track of moving targets and rapidly changing interference. However, we do not have access to either the SOI or the interference and we cannot use a pilot signal. Unique to our scenario is that the signal incident on the receiver—the input signal—is inaccessible and only a signal processed by the filter is usable. This scenario nullifies the use of traditional adaptive algorithms, which typically require pre-steering, training, or an input signal. Multipath effects are also significant in a dynamically noisy environment, which fluctuate and are highly unpredictable, preventing a device from distinguishing between the loss of signal (LOS) or some nth order multipath. As a result, we cannot make traditional direction-of-arrival (DOA) estimates. Because broadband noise can fluctuate wildly in frequency and direction, stochastic gradient method are also unusable; even if signals remain the same, no two measurements will be the same as a result of noise. This chapter investigates solutions to the scenario introduced above.

We first discuss the basic theory of beamforming and the unique challenges of broadband interference cancellation. Next, we present the requirements and challenges for building optical finite impulse response (FIR) filters, and review several innovative MPF designs including optical tunable delays and weighting schemes. We also review the state of the art optical beamformers recently proposed and experimentally demonstrated in literature. Furthermore, we detail a highly scalable photonic beamforming architecture designed for a particularly non-stationary, interfering environment. Finally, we introduce a specific application for the photonic beamformer namely, physical layer security in optical backhaul networks.

15.2 Primer on Antenna Arrays and Beamforming

Antennas arranged in some physical geometry—array—exploit the spatial relationship between the antenna elements to either measure or manipulate the spatial properties of RF signals which is also called beam steering. Typically, several antennas are located with uniform spacing of scale similar to the frequency of interest. If the signal source is far away from the antenna array, the beam can be considered as a plane wave with a wavefront orthogonal to the direction of propagation. This wavefront arrives at the antenna array at some angle, and as it propagates across the array it impinges upon each antenna with a delay experiencing a phase shift. The delay is related to both the angle of incidence of the beam and the physical layout of the array. The antenna array is able to resolve the signal's DOA by calculating the time differences between the responses of each antenna. This information can then be used to steer the beampattern. A signal processor can follow each antenna. The signal processor can be used to manipulate the signal in a useful way; that is, to suppress interferers and enhance the SOI.

More formally, consider an array of M antenna elements arranged in an xy plane. The DOA denoted by a monochromatic plane wave incident on the array is denoted as (θ, ϕ) where θ is the elevation angle measured from the z axis and ϕ is the azimuth angle measured from the x axis. The received signal at antenna m is transformed by the steering vector $\mathbf{a}(\theta, \phi)$ given by

$$a_m(\theta, \phi) = e^{j\omega\tau_m(\theta,\phi)}, \quad m = 0, 1, \ldots, M-1 \tag{15.1}$$

where ω is the signal carrier frequency, τ_m is the time delay associated with antenna m characterized by the array geometry. To implement beam steering, the array elements are weighted and summed. The incident signal $s(t)$ produces an output signal $y(t)$

$$y(t) = \mathbf{w} \cdot \mathbf{a}(\theta, \phi) \cdot s(t). \tag{15.2}$$

where $\mathbf{w}$ is the weight matrix vector which comprises of the complex coefficients w_m, and inner product $\mathbf{w} \cdot \mathbf{a}(\theta, \phi)$ is called the array factor $AF(\theta, \phi)$ [9].

To generalize, if the antenna array is receiving L signals $s_0(t), \ldots, s_{L-1}(t)$ with different DOAs $(\theta_0, \phi_0), \ldots, (\theta_{L-1}, \phi_{L-1})$, then the $M \times L$ steering matrix is

$$\mathbf{A}(\theta, \phi) = [\mathbf{a}(\theta_0, \phi_0) \ldots \mathbf{a}(\theta_{L-1}, \phi_{L-1})] \tag{15.3}$$

and the system output is given by

$$y(t) = \mathbf{w}^T \mathbf{A}(\theta, \phi) \cdot s(t). \tag{15.4}$$

If some of the signals are considered noise, the adaptive system becomes an optimization problem over the space of the M antenna weights. The weights can be chosen in such a way as to emphasize a signal coming from one direction while attenuating signals from other directions.

Consider the linear and circular antenna arrays shown in Fig. 15.4 which we use to illustrate the example of beam steering. The linear array consists of M antenna

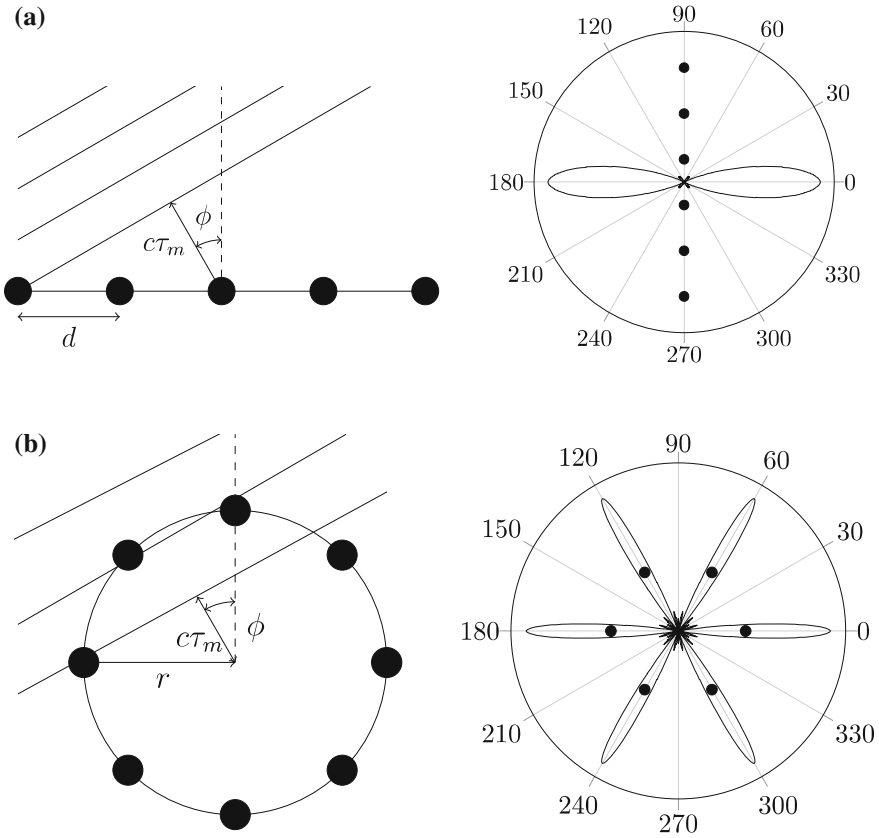

Fig. 15.4 **a** *Left* Linear antenna array for beam steering. Phase difference is found from distance $c\tau_m$. *Right* Response pattern of an unweighted linear array to a signal from different directions. **b** *Left* A circular antenna array. *Right* Response pattern of an unweighted circular array

elements equally spaced distance d apart arranged in a straight line along the y axis. If the first antenna element has phase 0, then the time delay to antenna m can be calculated by trigonometry to be

$$\tau_m(\theta, \phi) = m\frac{d}{c}\sin\phi\sin\theta \tag{15.5}$$

where c is the speed of light. The linear array with weights w_m then has an array factor

$$AF(\theta, \phi) = \sum_{m=0}^{M-1} w_m e^{j\omega m\frac{d}{c}\sin\phi\sin\theta} \tag{15.6}$$

which is comparable in form to the frequency response of an M-tap FIR filter: $F(\Omega) = \sum_{m=0}^{M} w_m e^{-jm\Omega}$. Hence, selecting weights for a particular spatial response is equivalent to selecting the weights of an FIR filter. The more popular circular antenna array can steer a beam in any direction. Here, the M antenna elements are arranged uniformly around a circle of radius r, with antenna 0 at $\phi = 0$. If the center of the circle has phase 0, then the time delay at each antenna element m is given by

$$\tau_m(\theta, \phi) = \frac{r}{c}\cos\left(\phi - \frac{2\pi m}{M}\right)\sin\theta \tag{15.7}$$

which gives a response of

$$AF(\theta, \phi) = \sum_{m=0}^{M-1} w_m e^{j\omega\frac{r}{c}\cos\left(\phi-\frac{2\pi m}{M}\right)\sin\theta} \tag{15.8}$$

15.2.1 Narrowband Beamforming

To use the antenna array to steer a signal, the complex weights at each antenna are adjusted to achieve the desired response. In the case of a narrowband signal, the weights can be simple phase shifts chosen to replicate a plane wave in the desired direction. These weights are pure phase delays, and can be realized with analog phase shifters attached to each antenna or with digital signal processing (DSP). Such a system is known as a phased array. For steering a beam with the linear and circular arrays, the weights are

$$w_m = e^{-j\omega m\frac{d}{c}\sin\phi} \text{ and } w_m = e^{-j\omega\frac{r}{c}\cos\left(\phi - \frac{2\pi m}{M}\right)}, \text{ respectively.} \tag{15.9}$$

Figure 15.5 illustrates an example of directional response of a steered circular phase array. Phase shift steering provides control over the direction of the main lobe which is centered on the look direction, but not over the relative placement of the smaller side lobes on other directions or nulls which are the minima of the response; signals from these directions are rejected by the array. To change the shape of the response, variable weights are applied to the phase shifted signals as shown in Fig. 15.6. An arbitrary phase shift is realized by adjusting the ratio between the original signals and a quarter-shifted copy of the signal [10]: $\Delta\varphi = -\arctan\frac{w_{m,1}}{w_{m,0}}$.

By controlling both the amplitude and phase of each antenna, this filter design implements weights as complex numbers. The complex weight vector $\mathbf{w}$ can be selected to solve the complex linear systems of (15.4) to achieve high gain of the SOI and suppression of the interference signals. The equation can be solved for up to $M-1$ interference signals which means the null steering array of M antennas can place up to $M-1$ nulls [3]. If there are fewer than $M-1$ interference signals, the additional degrees of freedom can be used to refine the gain levels and shapes of the side lobes. However, if there are more than $M-1$ interference signals, then the array cannot cancel them perfectly, but can still suppress them. In this case adaptive algorithms can be used to find the optimal weight vector for the incident signals. These standard optimization algorithms include gradient estimation, digital least mean square (LMS), and asynchronous LMS [11].

Filtering using phase shifts is only effective for narrowband signals, where the phase shift corresponds with the time delay between the antennas. For signals with different frequencies, the time delay between the antennas $\tau = d/c$ is constant, but the phase shift $\Delta\varphi_m = \omega\tau_m$ changes with frequency. A phased array therefore has a different response for each frequency and this is referred to as beam squint [4]. As a result, a broadband signal can get distorted after passing through the filter. To receive signals in a broad spectrum, the phase shifts can be replaced with TTDs

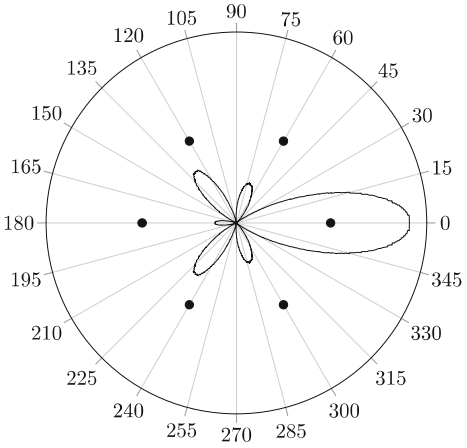

Fig. 15.5 Directional response of a circular phase array steered to angle 0. Power is depicted in linear scale

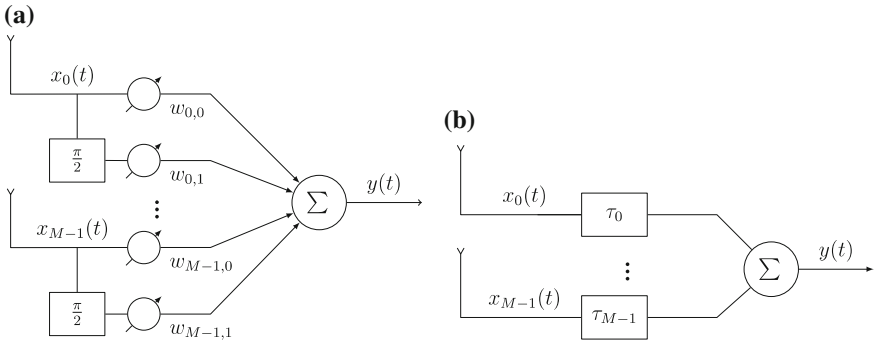

Fig. 15.6 **a** A weighted phased array beamformer applies both phase shifts and amplitude weights to alter the shape of the response pattern. **b** A delay-and-sum beamformer uses true time delays to receive a wideband signal

[12], as shown in Fig. 15.6b. A TTD can implement a phase shift greater than 2π for some frequencies, as required by extremely broadband signals. Then the spatial response is nearly the same for all frequencies.

Systems that use time delays for filtering are called delay-and-sum arrays. Digital receivers can trivially shift input signals using hardware shift registers or software signal processing. Optics is the perfect medium for creating TTD systems for broadband signals. Since optical beamforming is based on using fiber optics or other types of discrete optical components that already exist in current broadband optical networks, they are by nature broadband. TTD filters work well for receiving broadband signals, but they only filter in the spatial domain. For interference signals at different frequencies, it would be useful to control the frequency response as well —wideband beamforming. In this chapter, we will focus on photonic broadband beamformers.

15.2.2 Wideband Beamforming

For wideband arrays, it is desirable to control not only the spatial response but also the frequency response. To achieve an arbitrary frequency response, the weights w_m are replaced by linear filters $h_m(t)$ with frequency response $H_m(\omega)$. The combined spatial and frequency of the system is the sum of the filtered array factors from (15.8)

$$P(\omega, \theta, \phi) = \sum_{m=0}^{M-1} H_m(\omega) e^{j\omega \frac{r}{c} \cos\left(\phi - \frac{2\pi m}{M}\right) \sin\theta}. \tag{15.10}$$

A signal whose frequency and direction of arrival falls near the peak of (15.8) will be amplified whereas the one near null will be rejected by the filter. In the

adaptive array proposed by Widrow et al. in 1967 [10], the filters were analog tapped delay lines (TDLs).

TDL filters, also known as transversal filters [13], are the continuous-time analogue of the well-known discrete-time FIR filter. As shown in Fig. 15.7, the input signal is delayed by successive time intervals, called taps. These delayed signals are then weighted and summed. For an N-tap filter with weights w_n and a constant delay T_d between each tap, the output is given by

$$y(t) = \sum_{n=0}^{N-1} w_n(t) x(t - nT_d) \tag{15.11}$$

and the frequency response is

$$H(\omega) = \sum_{n=0}^{N-1} w_n e^{-j\omega n T_d}. \tag{15.12}$$

Note that both the frequency response of the TDL filter (15.12) and the spatial response of the phase array (15.8) have a similar form to an FIR filter. Hence, in the most general terms, the physical formation of the antennas provides spatial filtering while the filters provide frequency filtering. By changing the weights of the FIR filters, one can manipulate a beamformer to act as a spatial and frequency filter and change the sensitivity of the beampattern to different frequencies and angles. Mathematically, if an N tap filter is used for each of the M antenna elements in the array, then there are MN total weights and delays in the system. The overall response of the array is found by substituting (15.12) into (15.10):

$$P(\omega, \theta, \phi) = \sum_{m=0}^{M-1} \sum_{n=0}^{N-1} w_{m,n} e^{-j\omega\left(nT_d - \frac{r}{c}\cos\left(\phi - \frac{2\pi m}{M}\right)\sin\theta\right)}. \tag{15.13}$$

The task of beamforming is to select the optimal set of MN weights to achieve the desired shape of $P(\omega, \theta, \phi)$. Figure 15.8 shows the simulation response of a

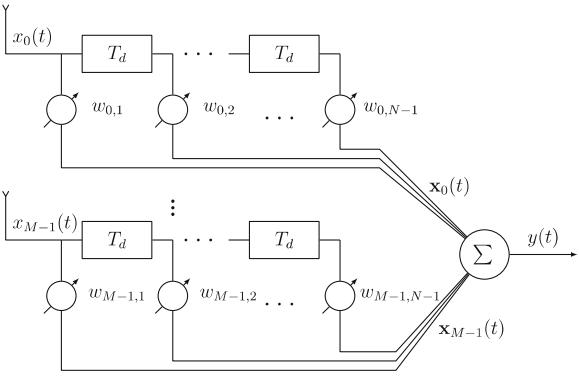

Fig. 15.7 Antenna array with tapped delay line filters

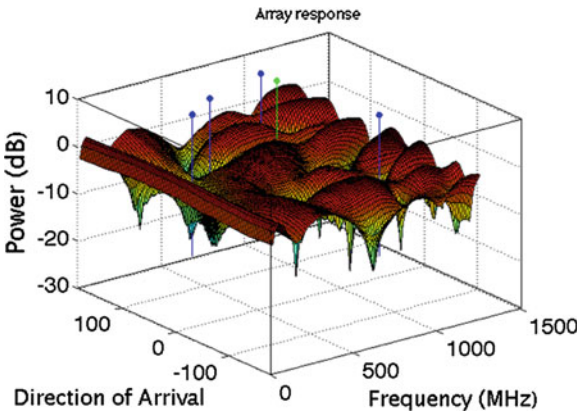

Fig. 15.8 Simulated spatial and frequency response of a tapped delay line filter using arbitrary weights

wideband 4-antenna, 8-tap circular beamformer. The beam pattern for a system with SOI of 500 MHz at 90° and interferences at 900, 1000, and 300 MHz at 120°, −70°, and 60° respectively demonstrates both the spatial filtering on the *x*-axis and the frequency filtering on the *y*-axis. We notice that nulls occur at the interferers while there is a peak at the SOI frequency and angle.

15.3 Microwave Photonic Filters

The previous section introduced the FIR filter as a TDL architecture. This section details the requirements and challenges for building *optical* FIR filters. We also review several innovative MPF designs including optical tunable delays and weighting schemes proposed and experimentally demonstrated in literature.

Optical filters or microwave photonic filters, are photonic subsystems specifically designed with the objective of carrying out the same functions as those of electronic or digital filters within the microwave range in an RF system or link [5]. The unique properties of MPFs offer many advantages, including high bandwidth, low loss across the entire bandwidth, reconfigurability, and immunity to EMI. Thus, there has been a considerable interest in the field of photonic signal processing for microwave filtering applications. Traditional RF and electronic approaches cannot practically handle wide bandwidths in the GHz range, whereas processing in the optical domain takes advantage of the broadband capabilities of optical delay schemes. Optical filters require only a single set of equipment to be able to cancel across a huge band of frequencies. Consequently, optical systems can potentially offer SWAP advantages, that is, savings through size, weight, and power. This is particularly critical for field-tested military or aviation applications where size and power are of key importance.

In this chapter, we are specifically interested in the possible application of MPFs in photonic phased array antennas, where they can provide the capability of steering

without any physical movement, and offer the ability for precise spatial and frequency control of broadband signals. The key-motivating factor is that MPFs are easily tunable and reconfigurable in real time, allowing for filtering with adaptive capability. One can leverage these properties when designing such a system. Moreover, the field of photonic TTD units is essential for transversal, FIR filters (in phased array antenna systems) as it allows for wide bandwidth signal processing with little or no distortion or pulse broadening without being limited to a 'design frequency'. MPFs are the perfect optical complement for frequency filtering to the spatial filtering of RF antenna arrays.

15.3.1 Requirements for MPFs

From (15.11), an FIR filter is also a TDL filter. In order to replicate the equation, we need to be able to complete the same mathematical operations using optics. Each tap of an FIR filter is a weighted delay—methods for optical weighting and optical delay lines are necessary. The weighted delays are summed together to complete the FIR filter, so an optical method of adding the symbols together is also needed. All optical (and even analog) based filters require these three components: *optical weights*, *optical delay lines*, and a *summation method*. Traditional optical fused couplers are built specifically for the purpose of combining optical signals (and their powers), and since they are used widely in any optical communication system, we will focus on optical methods for delays and weights here.

Figure 15.9 shows a general reference layout of an MPF. In all optical filters, the RF signal must be converted to an optical signal. Generally, a continuous-wave (CW) laser source modulates the RF signal onto the optical domain using modulators such as electro-optic modulators (EOMs) like the Mach-Zehnder modulator (MZM), or electro-absorption modulators (EAMs). The optical signal is then fed

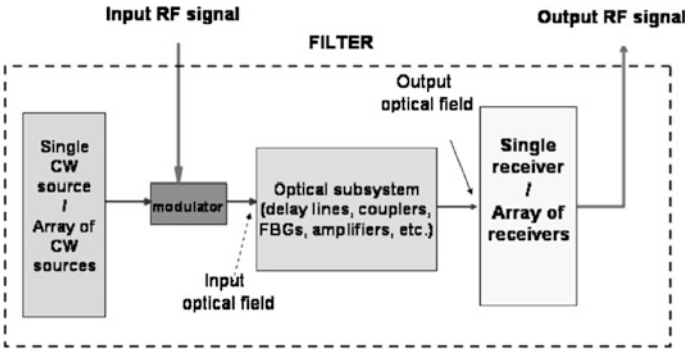

Fig. 15.9 General reference layout of a microwave photonic filter showing the relevant electrical and optical signals [5]

into a photonic circuit that delays and weights the signal on parallel taps and then combines them with a fused coupler (or other method). The optical signal can be converted back to an electrical signal using a photodetector.

15.3.2 Popular MPF Architectures

Many optical tunable delays and innovative weighting schemes have been proposed and experimentally demonstrated in literature. We review some of the popular techniques and present two unique MPF architectures.

Popular optical delaying techniques include filters that use fiber-Bragg gratings (FBGs) to delay filter taps [14]. Delays are created by forcing the optical signals to propagate along the FBG until reflected by a wavelength-specific grating. FBGs are popular since a whole array can be fabricated onto a single piece of optical fiber. Fiber delay lines have also been proposed for TTD in MPFs [15, 16], but are bulkier than FBG-based delays when filter taps become large.

Fully tunable and programmable weighting using free space methods such as spatial light modulators [17] and multi-port programmable wavelength processors [18] have been demonstrated. Unfortunately, typical optical systems are generally limited to positive tap coefficients, as light intensities are intrinsically "positive". Therefore, the shapes of their transfer functions are severely constrained and can only be used to implement low-pass filters (LPFs). The addition of negative coefficients in filter schemes allows for a practical filter with passband capabilities [5].

There are many ways to create negative optical weights. Recent advances in negative coefficient weighting have used cross-phase modulation (XPM) in an semiconductor optical amplifiers (SOA)-MZ interferometer [19] and self-wavelength cross gain modulation (XGM) in an SOA [20], but are suitable only for realizing a few taps. Another technique involves using multiple phase inversion in an SOA-based XGM wavelength converter [21]. An innovative method involving sinusoidal group delay gratings, which use FBGs to achieve positive/negative weighting and delays was proposed in [22].

Weight and delay are 'coupled', and it is difficult to have freely tunable attenuation without affecting the delays. Other optical weighting schemes involve polarization modulation and optical polarizers [19, 23]. While these approaches are simple, scalable, and tunable, the method relies heavily on mechanical polarization controllers, which cannot rapidly change the polarity of the taps (to sub millisecond-length time).

Simpler techniques entail using the negative bias slope of MZM to π-shift the output to create negative coefficients [24–27]. However, some techniques necessitate using two MZMs, which can be bulky when scaled [24]. Others using one MZM rely on the dependence on wavelength but positive and negative coefficient outputs are of different power. A novel technique using a specially designed integrated 2 × 1 MZM to achieve π-shifting was introduced in [26]. On the other hand,

a simple technique using a 1 × 2 dual output MZM to achieve negative weighting by using phased-inversed dual outputs was proposed in [27].

Figure 15.10 shows an example of MPF using a spectrally-sliced free-space configuration [5]. The most distinctive and important part of the setup is the optical tapping through a sliced broadband source. A broadband laser is sliced by a diffraction grating into 10 different wavelengths. The slicing into individual wavelengths allows summing to be done incoherently. Use of spatial light modulators achieves the weighting and delaying of the samples. Fast tunability can be achieved as individual spatial light modulators (SLMs) can be turned ON and OFF, which are used to eliminate specific spectrum slices.

Figure 15.11 shows another realization of a MPF employing a discrete time optical transversal filtering scheme [28]. The unique characteristic of this system is the pulsed laser source being used. This means that the optical pulses sample the RF

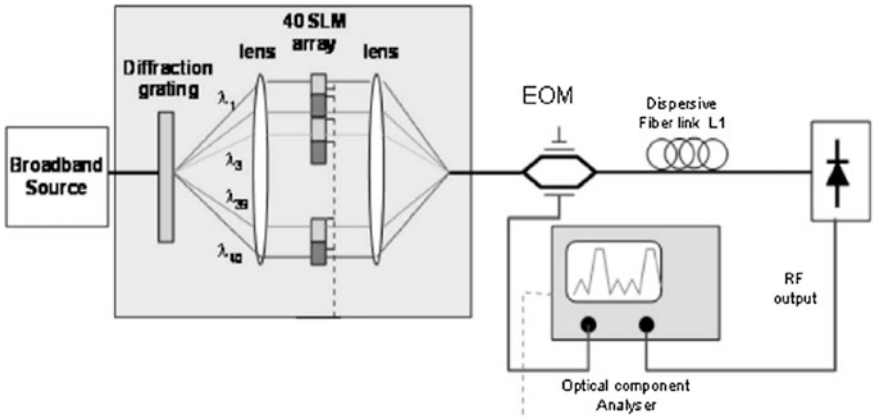

Fig. 15.10 Transversal MPF using spectrally-sliced free-space optics [5]

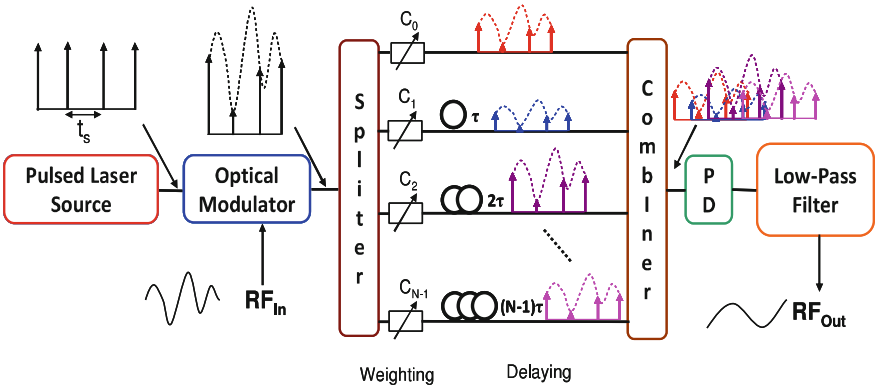

Fig. 15.11 Discrete time optical transversal MPF [28]

input data (discretely). There is no need to have a separate analog-to-digital converter (ADC) as the laser source serves that role. The delay is achieved through fiber delay lines. In order to avoid coherent summing, the delays are chosen so that no optical pulses from one tap overlaps with pulses from another tap. Optical attenuators provide weighting. There are no negative coefficients in this scheme.

15.3.3 Optical Technologies for MPFs

We now present the state of the art optical components and techniques that are employed in MPFs. As stated earlier, MPFs need an optical delay scheme and also an optical weighting scheme complete with negative coefficients. For an adaptable filter, tunability of (at least) the weights is required which need to be electronically programmable so that they can be quickly tuned. Table 15.1 summarizes some of the novel optical components used for optical delays or weights in MPFs from recent literature.

FBG arrays can be used for creating compact but fixed delay lines [29]. The drawback is that the fixed delays prevent reconfigurability of the filter bandwidth. Furthermore, this approach employs a spectrally sliced broadband amplified spontaneous emission (ASE) noise source. While slicing this source will create multiple optical filter taps, the ASE source is fundamentally noisy. An improvement

Table 15.1 State of the art optical technologies for microwave photonic filters

References	Functionality	Technology	Advantages	Limitations
[29]	Optical delays	FBG arrays	No need to use bulky and slowly tunable fiber delay lines	Spectrally sliced broadband ASE noise source; hard to tune and reconfigure
[30]	Optical delays	WDM filter with FBG arrays	WDM system, implementation of negative coefficients	No tunability/ programmability of delays
[31]	Optical delays	WDM filter with chirped FBG arrays	WDM system, reconfigurable bandwidth	No negative coefficients; lacks easy tunability/ programmability of weights
[17]	Optical weights	Spatial light modulators	Programmability of weights	Free space optical setup (not compact); spectrally slice a noisy ASE source
[18]	Optical weights	Liquid crystal on silicon	Programmability of weights	Free space optical setup (not compact); spectrally slice a noisy ASE source
[27]	Optical weights and delays	1 × 2 MZM	Simple implementation of negative weights, delay using FBG arrays	Spectrally slice a noisy ASE source; lack *easy* tunability/programmability of weights

can be achieved by using a wavelength-division multiplexing (WDM) scheme paired with FBG delay lines [30]. This technique uses an array of distributed feedback (DFB) lasers for the optical taps. While this gives the filter more dynamic range, it sacrifices simplicity and also lacks tunable delay lines. In contrast, using chirped FBGs with tunable DFB lasers allows controllably variable delay lines [31]. However, this technique does not incorporate negative coefficients.

Similarly, many technologies have been developed for optical weighting schemes. Free-space weighting schemes have recently garnered popularity including the weighting technique based on SLM [17] and liquid crystal on silicon (LCOS) [18]. Both these methods are extremely precise, can scale to filter orders of hundreds, and are easily programmable. However, they still have a couple of drawbacks. Firstly, they are free space optical techniques that are bulky and occupy a much larger footprint than discrete optics. Secondly, they lack the ability to create negative coefficients. A simple and compact method for creating negative coefficients can be integrated into the modulators that convert the electrical signal to the optical signal [27]. However, this negative weighting technique must be combined with another set of tunable optical weights for programmability.

15.4 Photonic Adaptive Beamformers

In this section, we first review the state of the art optical beamformers recently proposed and experimentally demonstrated in literature. We also detail a highly scalable photonic beamforming architecture designed for a particularly non-stationary, interfering environment. Finally, we introduce a specific application for the photonic beamformer namely, physical layer security in optical backhaul networks.

Beamformers have attracted significant interest because of their wide range of applications from radar, communication, and sensing. Beamforming is a technique that utilizes an array of antennas as a spatial and frequency filter to manipulate the beampattern to maximize the SNR of the SOI while cancelling/suppressing interferers and noise without a priori knowledge [32]. For instance, a beamformer can spatially separate two signals that have overlapping frequencies but originate from two different spatial locations [33]. Beamformers use optical FIR filters to process the signals temporally with thermo-optic optical attenuators—controlling the signal amplitudes and delays from each antenna element—to adaptively and rapidly adjust the beampattern; that is, the whole array can act in unison to steer the beam pattern. Meanwhile, the geometric configuration of the antennas allows the signals to be processed spatially. This makes beamforming attractive for overcoming the directivity problems of a single antenna while offering a higher gain [3]. Adaptive beamformers are particularly crucial in applications involving a highly non-stationary target environment. Compared to conventional RF beamformers which have limited narrowband performance due to their reliance on electrical phase shifters, the wideband nature of optics offers a clear advantage. The architecture also offers the

distinct advantage of scalability to hundreds of antennas, as needed for practical systems.

The first adaptive beamformers were used as self-phased antennas that reradiated signals in the direction in which they were received without prior signal knowledge. In the 1960s, Howell and Applebaum introduced their versions of adaptive antennas for interference nulling [3]. Widrow followed closely with self-optimizing adaptive algorithms [10]. Applebaum and Widrow focused on beamforming specifically for applications in the field of sonar and radar signal reception. Seismic array development was especially popular in the 1960s. Recently, the major area of interest is radar and communication systems for interference suppression [3]. Direction finding in severe interference environments has also been a popular topic, as is scanning for high angular resolution imaging. We will focus on interference cancellation techniques in this section.

15.4.1 State of the Art Photonic Beamformers

This section provides a review of the recently demonstrated state of the art optical beamformers in literature. As explained previously, a photonic beamformer is an array of antennas with a set of *optical signal processors* attached to each antenna. In the previous section we stipulated the requirements needed for an FIR filter: a method for creating both optical delays and optical weights. The same requirements are necessary for a photonic beamformer. Moreover, optical delays with TTD capability is essential for a beamformer, as explained in Sect. 15.2. However, since a beamformer consists of multiple FIR filters (one for each antenna), scalability with optical components is very important as well. We focus the literature review on methods for TTD optical beamformers with an emphasis on scalability.

Figure 15.12 shows a TTD beamformer architecture based on FBG prisms. FBG arrays are created in a prism format in which different sets of delays (five as depicted in the figure) are selected for a specific wavelength of a laser. The FBG prism is built so that the delays create a pre-steered beamformer [34]. However, this architecture cannot be fully tunable, as the number of pre-steered directions is limited by the number of FBGs etched in the array.

A similar approach but that is tunable is shown in Fig. 15.13. In this scheme, instead of FBGs, the beamformer uses dispersive fibers that can be precisely tuned by a finely tunable laser [35]. However, this method, while more precise, is inherently slowed by the tuning speed of the laser.

Figure 15.14 depicts a scheme for a TTD beamformer based on WDM demultiplexer (demux) delays [36]. The architecture consists of a single antenna, a tunable laser with 8 λ's, and a corresponding WDM demux which selects one of eight possible delays. The limitation in its resolution depends on the tunable laser and the amount of wavelengths supported by the arrayed-waveguide (AWG) demux.

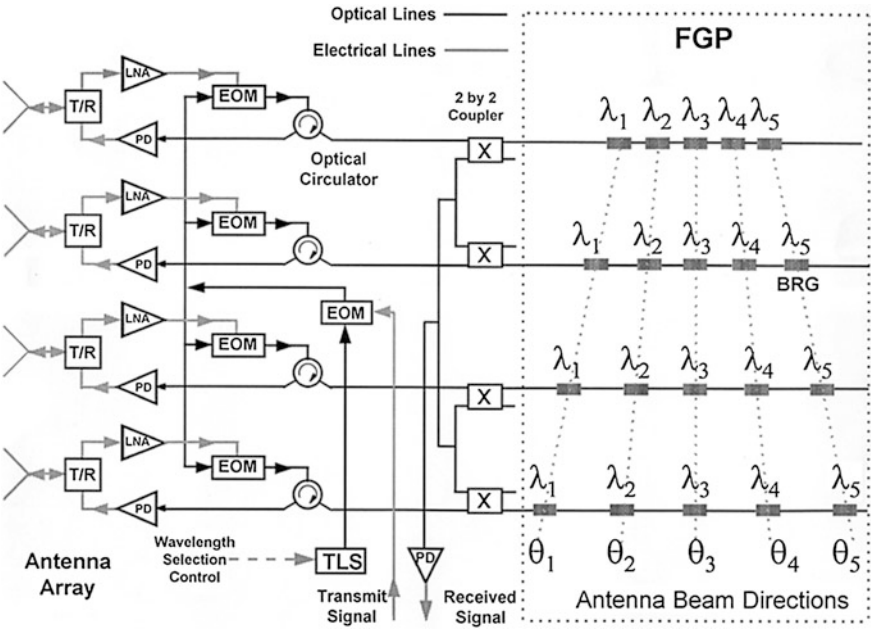

Fig. 15.12 Beamforming architecture based on FBG prism [34]

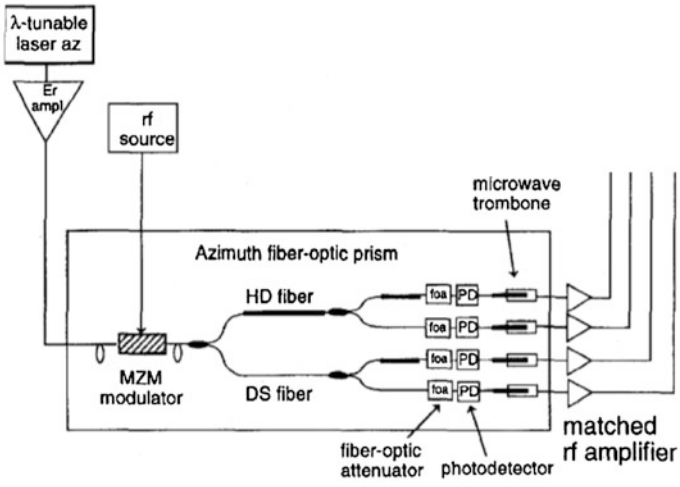

Fig. 15.13 Beamforming architecture based on dispersive fiber prism [35]

Furthermore, the number of lasers required scales linearly with the number of antennas, which can become bulky with large beamforming systems that necessitate hundreds of antennas.

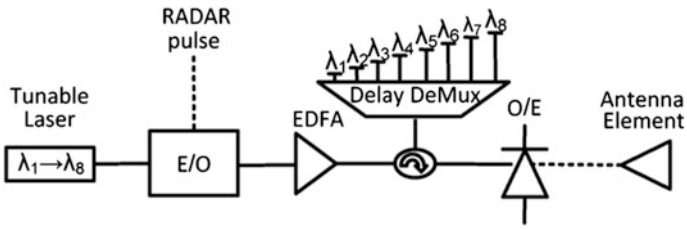

Fig. 15.14 Beamforming architecture based on WDM demux delay lines [38]

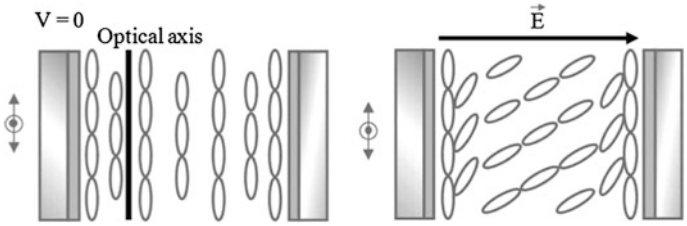

Fig. 15.15 SLM delay lines [37]

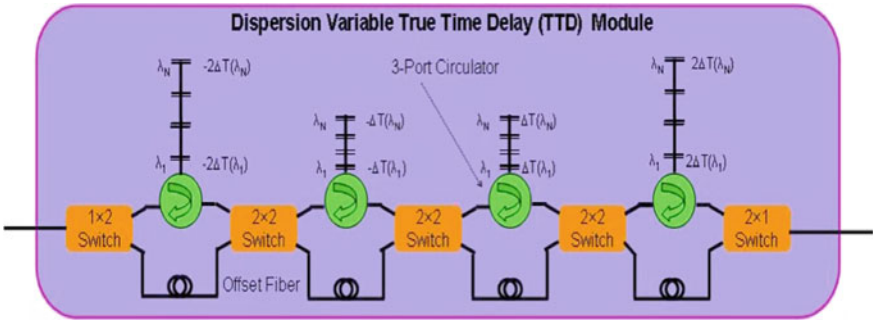

Fig. 15.16 Bit-switched delay lines [41]

Antenna arrays that use SLMs to perform optical delays have also been proposed [37]. By apply an external electrical field as shown in Fig. 15.15, dielectric molecules in the SLM form different polarizations. The polarization changes the index of refraction of the delay line which affects the length of time the light travels through the device.

Photonic crystal fiber and XGM in SOAs have also been used to create TTD lines in photonic beamformers for multi-transmit systems [38, 39]. On the other hand, bit-switched delay lines are also popular [40, 41]. Figure 15.16 shows an example of bit-switched delay line that selects a particular delay from a chain of FBG arrays using a tunable laser.

A beamforming architecture based on opto-VLSI is shown in Fig. 15.17 [42]. The opto-VLSI processor is an array of liquid crystal (LC) cells driven by a Very-Large-Scale-Integrated (VLSI) circuit. Delays can be created for each antenna by slicing a broad-band optical source (ASE-based source) and routing specific sliced wavebands through the Opto-VLSI processor to a high-dispersion fiber [42].

A beamforming architecture based on high dispersion fiber has also been reported [43]. Here the beamformer uses an array of lasers that each experiences a different delay based on passing through a wavelength-dependent high dispersion fiber. Figure 15.18 depicts the architecture of a single antenna. By using two π-shifted EOMS, negative coefficients can also be implemented. However, this technique requires a laser array for *each* antenna array.

Recently, the integration of the photonic components into an integrated *beam-former-on-chip* has been explored [44, 45]. Next generation systems investigate a scalable integrated photonic beamformer that can be electronically controlled for adaptive interference cancellation. The possibility of creating a beamformer-on-chip has become a question of not "if" but "when". Figure 15.19a illustrates an integrated beamformer. Figure 15.19b shows a 16-antenna beamformer integrated on a chip, roughly the size of a 20-cents of an euro coin. These systems show the potential for extreme savings in SWAP along with full broadband processing ability.

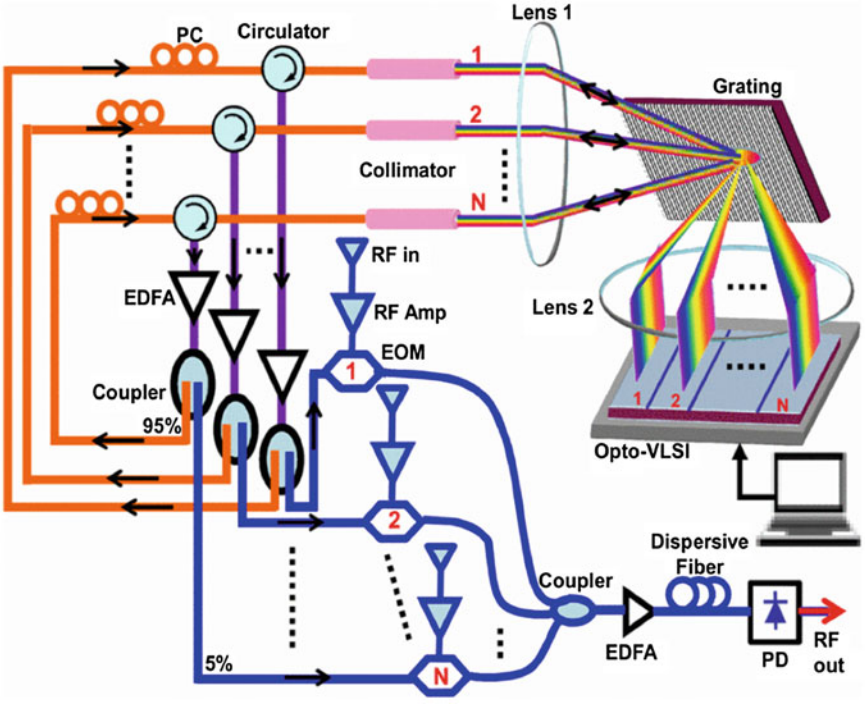

Fig. 15.17 Beamforming architecture based on Opto-VLSI [42]

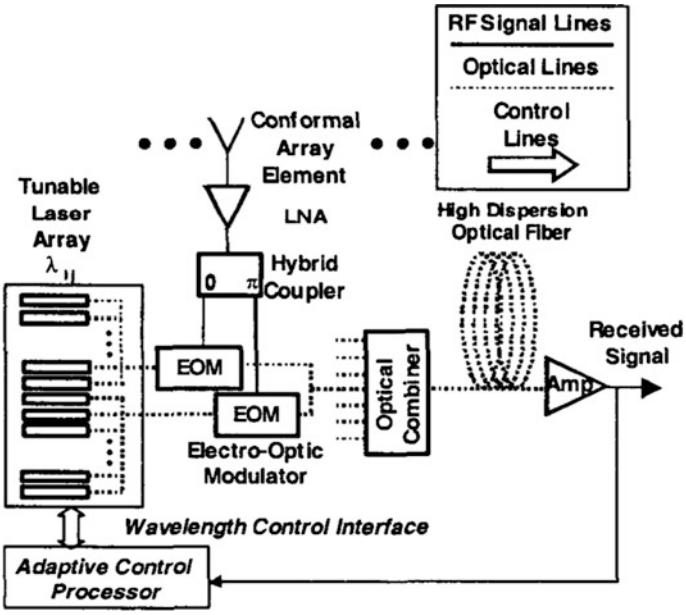

Fig. 15.18 Beamforming architecture based on high dispersion fiber [43]

15.4.2 Highly Scalable Adaptive Photonic Beamformer

The key characteristic of a reconfigurable and tunable photonic beamformer is scalability. Thus far, most of the beamformer architectures reviewed, are not scalable to large arrays—the number of lasers required by these systems increases linearly with the number of antennas. In this section, we present a highly scalable photonic beamformer [46], unique to our lab, which is specifically designed for a particularly non-stationary, interfering environment. Using optical transversal filters for each antenna element and thermo-optic optical attenuators, the array is capable of both spatial beamforming and frequency-domain filtering while adaptively and rapidly adjusting the beampattern. Our architecture offers the distinct advantage of scalability to hundreds of antennas, as needed for practical systems, by using a novel single-mode to multimode (SM-MM) combiner, and the same set of laser wavelengths can be used for every antenna in the system. By eliminating coherent effects, our system uses the same fixed set of optical wavelengths for each antenna in the system, resulting in a simple and compact architecture. We present experimental results to show proof-of-concept and demonstrate the proposed adaptive beamformer performance.

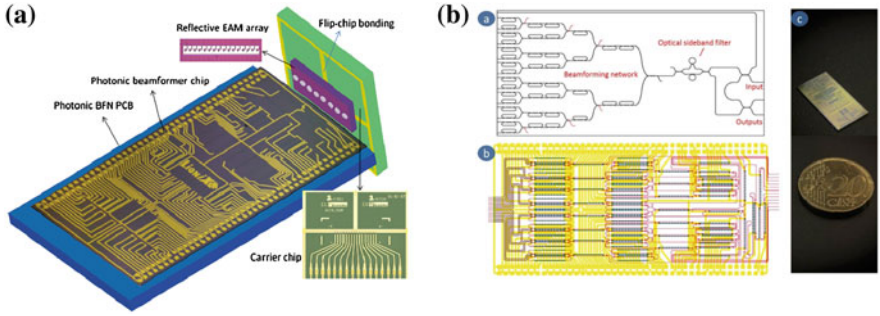

Fig. 15.19 **a** Potentially integrated beamforming network with EAM array [44]. **b** Schematic of 16 × 1 beamforming network with chip mask layout and photograph of a fabricated chip [45]

15.4.2.1 System Overview

Figure 15.20 shows the architecture of a wideband photonic beamformer that we recently demonstrated experimentally. The key component of the beamformer is the optical transversal filter which is driven by two eight-channel DFB laser arrays. The first array of wavelengths λ_{1-8} corresponds to the positive coefficients whereas the second array of wavelengths λ_{9-16} corresponds to the negative coefficients. The optical sources are inserted into a compact 16-channel thermal-optic attenuator for easy adaptive control of the weights through a computer or voltage source. The attenuators have a response time of 10 μs per 0.1 and a 20 dB range.

The weighted taps are then combined using an AWG multiplexer (mux). The RF signal to be processed is modulated onto the optical carrier using a dual output electro-optic MZM. The modulated signals of the outputs are biased at the inverse, π-shifted, parts of the modulator transfer function. We use this complimentary output to implement negative coefficients. Both outputs have equal insertion losses of 3.7 dB. The weighted signals exit from both the positive and negative outputs of the MZMs. The complementary outputs are launched in FBG arrays that only reflect and delay the wavelengths assigned to the respective coefficients, via an optical circulator (OC).

The coefficients encounter FBGs with the same delays, but at different wavelengths. As a result, each delay has both a positive and negative tap, and the attenuators are used to switch on the tap and weight each tap by enabling/disabling a certain wavelength. In this way, our 16-wavelength filter provides eight positive/negative taps. Since time delays and filter bandwidth are inversely proportional, fabricating FBGs with closer spacing and shorter delays can increase bandwidth.

There is a total optical insertion loss of ∼19.5 dB for each filter. If each DFB laser has 13 dBm of power, each filter receives 9.4 dBm of power after splitting to four antennas and outputs −10.1 dBm into the combiner. Assuming a four-antenna beamformer, −4.6 dBm of power finally reaches the high speed MM photodetector, well above the −25 dBm limit.

The outputs of the optical filters are summed using a special SM-MM optical combiner, as in Fig. 15.20. The architecture is a blind adaptive approach, in which the adaptive algorithm only has access to the output of the system. This requires a single conversion to RF at the output, whereas traditional systems require an ADC for each antenna element, which is impractical for large antenna systems. As a result, conventional criteria such as minimum mean square error (MMSE) cannot be used and analytical Wiener solutions cannot be found. Instead, blind algorithms rely on correlating the processed signal with some known characteristic of the signal of interest (such as frequency), and applying a gradient-based algorithm.

Our main advantage is that the same set of 16 wavelengths is used for each antenna, reducing complexity and increasing scalability. Typically, when signals of the same optical wavelength are combined, beat noise from coherent summing will occur and severely degrade the performance. Therefore, without the use of a SM-MM combiner the architecture would require 16 lasers for each antenna. To re-use the same wavelengths, the SM-MM combiner is used. The combiner couples signals from several individual single-mode fibers to distinct modes inside a multimode fiber. The combiner offers the advantage of phase-insensitivity and coupling without optical interference. In-depth information and experimental data demonstrating operation can be found in [47].

The architecture scales by simply adding optical splitters and amplifiers up to the limit imposed by the ASE of the amplifiers. The optical weights, which are integrated sixteen per chip and electrically controlled, do not limit the scalability of this

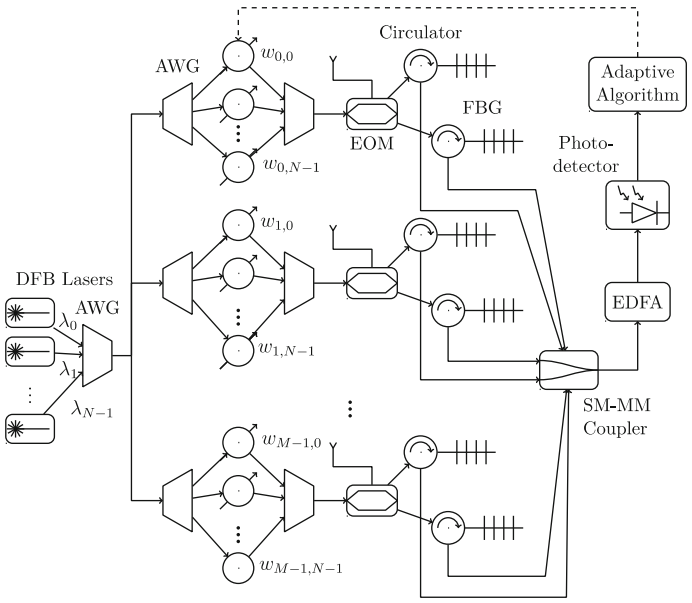

Fig. 15.20 Highly scalable photonic beamformer architecture ($N = 16$, $M = 4$)

architecture, nor does the addition of FBGs. A 100 μm multimode fiber can accept up to 113 inputs (or antennas).

15.4.2.2 Proof-of-Concept Experimental Results

We experimentally demonstrate an 8-tap filter with tap weights [1.0914 1.0617 −1.0715 −1.0814 −1 −0.9683 0.9795 0.0594] and delays incremented by 4 ns. The dark blue dotted curve in Fig. 15.21 shows the theoretical values and the thick light green curve shows the measured magnitude response. We are able to achieve a maximum extinction ratio of ∼40 dB. The bandwidth and the depth and placement of the notches depend on the precision of both the delays and weights. Moreover, our optical system adds no additional noise to the processed signal, as seen in Fig. 15.21.

The data shows a 4.5 dB loss associated with the architecture. RF systems in the low GHz range exhibit typical losses around 1 dB. RF systems in the high GHz range (60 GHz), an area in which photonic systems are expected to excel, exhibit ∼35 dB loss with one filter and a ∼17 dB loss with a four-filter beamformer [48]. RF signal losses in optical systems in general originate from the electrical-to-optical conversion efficiency of the modulators and the modulation depth of the signal during this conversion. To reduce loss further, removal of the optical dc level of the processed signal would allow the signal to be optically amplified further, reducing the system insertion loss.

We experimentally demonstrate an adaptive single-antenna beamformer consisting of 8 fully tunable taps with fixed delays of 400 ps and a bandwidth of 2.5 GHz. We employ a modified version of the LMS algorithm called block LMS with a block size of 256 and stepsize of 512. The adaptive results are preliminary. The authors only had access to a single 5 Gs/s ADC card, instead of the two required for the LMS algorithm.

A signal generator is fed into two narrowband tones at 200 MHz and 1 GHz to the filter. The algorithm is programmed to cancel the 1 GHz interference and pass the 200 MHz signal. Our workaround involves only digitizing the filtered output signal. The input signals are replicated digitally and are used to calculate the error signal. The adaptive algorithm then calculates optical weights that are sent to the attenuators. We observe an SIR (signal-to-interference ratio) improvement of ∼20 dB after ∼60 iterations at the output of the filter. We are able to drop the interference to just 5 dB above the noise floor. The results are good and can be easily improved with a second digitizer. In the future, we plan to apply a blind adaptive technique as described previously. Limited resolution associated with the optical attenuators degrades performance.

Future work will include the construction of multiple transversal filters to complete true spatial beamforming capability.

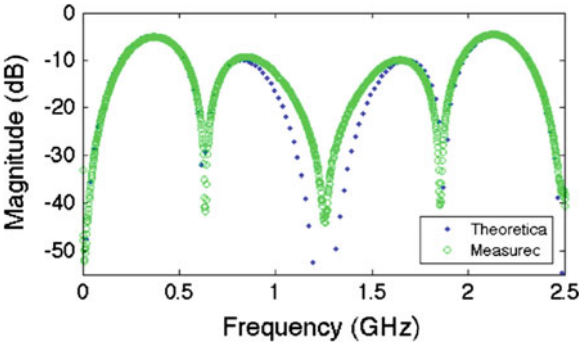

Fig. 15.21 Measured and predicted magnitude response of eight-tap FIR filter

15.4.3 Photonic Beamforming for Physical Layer Security

We introduce a specific application for using the photonic beamformer—physical layer security in optical backhaul networks. The purpose of this section is to demonstrate the applicability of the beamformer in commercial systems and to test the capabilities of the beamformer.

Emerging mobile services, such as mobile banking and desktop-to-mobile applications, require both increasingly high data rates and high data security. To address the rising bandwidth demand, strong emphasis is being placed on fiber-optic back- and fronthaul of mobile data [49–51]. While optical architectures that can satisfy the required data rate and latency requirements have matured [52–58], enhancing data security via optical-layer techniques is still in its infancy [59–66]. The potential of such physical-layer security is tremendous. For example, while higher-layer approaches, such as encryption or steganography, can be cracked by malicious eavesdropping, optical-layer techniques can prevent eavesdroppers from physically receiving the signal in the first place. The highest form of security thus resides in the physical layer, rendering it attractive for data-sensitive mobile fronthaul applications.

To implement security on the physical-layer, photonic beamforming can be used in the optical fronthaul network to cancel the signal (i.e. create a signal null) in the physical direction of an eavesdropper. For the downlink, this can enable sensitive data to only be received by an intended user within a meter-scale radius, based on the intended user's spatial location and signal carrier frequency. Given the user's spatial/frequency coordinates, a photonic beamformer can create the desired signal null by effectively manipulating a beampattern that propagates through the optical fronthaul network. This is achieved by the beamformer's array of RF antennas and a series of adaptive optical FIR filters. The physical formation of the antennas provides spatial filtering while the FIR filters provide frequency filtering. By changing the weights of the FIR filters, an adaptive beamformer that can respond to dynamically-changing/noisy environments can be implemented. Similarly, physical-layer security can also be provided on the uplink side, with potential application in a shared, multi-operator environment. In this case, various signals picked up by remote antennas can jointly

propagate through a shared fronthaul infrastructure and be securely separated on a per-operator basis via adaptive photonic beamforming at a centralized processing site. It is noted that the proposed optical-layer security approach is also transparent to the modulation format of the underlying wireless signal.

To the best of our knowledge, we have proposed and demonstrated the first experimental adaptive photonic beamforming technique for physical-layer security in optical fronthaul of mobile traffic, achieving up to 43 dB signal cancellation of an undesired eavesdropper and 30 dB power budget over 8 km standard single mode fiber (SSMF) fronthaul distance. The proposed approach is attractive for secure optical fronthaul of advanced mobile services and is transparent across heterogeneous mobile technologies and standards.

15.4.3.1 Experimental Setup, Results, and Discussion

The proposed fronthaul architecture using photonic beamforming in the downlink and the uplink is shown Fig. 15.22. In both cases, the beamformer acts as an optical spatial and frequency filter that preserves optical signals arising from desired physical orientations and carrier frequencies, while canceling signals from undesired physical directions and frequencies. In the downlink, mobile data signals from a centralized site are applied to parallel optical adaptive FIR filters, which optically modulate and filter the input. The processed optical signals are then transmitted over parallel SSMF optical fronthaul links to an array of remote antennas. The optical FIR filters and remote antenna array together form the beamformer. Specifically, by proper assignment of the beamformer's filter coefficients, the remote antennas are turned into a distributed spatial filter that directs the output only to intended users. The configuration of Fig. 15.22a can thus be used to securely deliver data to users 1 and 3 while producing a null in the direction of user 2, or vice versa. In the uplink in Fig. 15.22b, wireless signals from multiple users are first detected by the remote antenna array, and optically processed by the FIR filters such that, after SSMF transmission and photodetection, only the signal from intended users (e.g. user 1 and user 3) is delivered to the centralized site, while undesired interferers are suppressed (e.g. user 2).

For downlink experiments, 2.5 and 5 GHz sinusoids are used as the SOI to be directed by the photonic beamformer to an intended user. After SSMF transmission and photodetection, the received SOI power is measured at both intended user and eavesdropper locations, mutually separated by 0.5 m. Downlink beamformer performance is thus measured in terms of the signal strength ratio (SSR) at different user locations. The beamformer is adjusted for maximum cancellation. Figure 15.23 shows the SSR for the 2.5 and 5 GHz signal. Similarly, for uplink measurements, 2.5 or 5 GHz sinusoids are used as the SOI, while a sinusoid at 900 MHz emulates an interferer to be suppressed. The two wireless RF signals are generated at different locations (0.5 m separation), picked up by the antenna array, processed by optical FIR filters, propagated over parallel SSMFs, combined using a SM-MM coupler, and detected by a multimode PD. In the uplink, the SSR of the SOI versus the

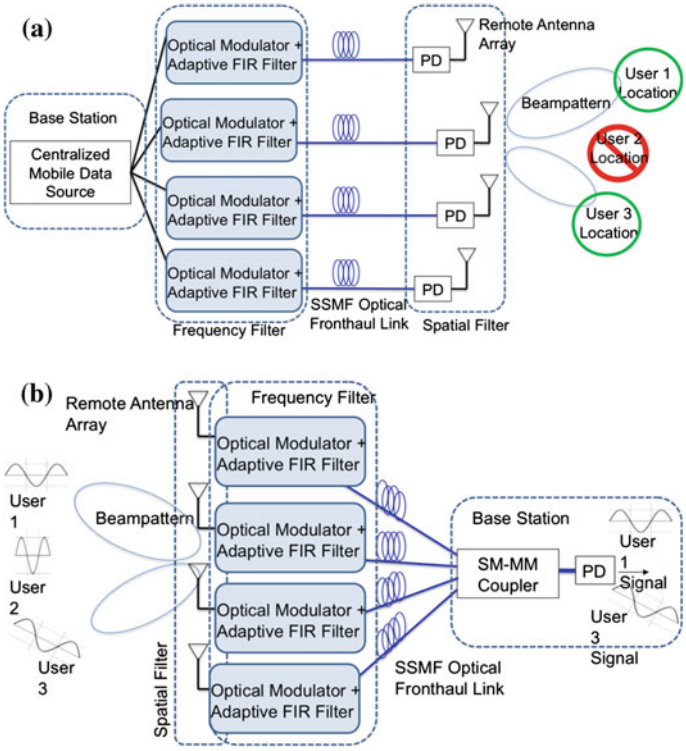

Fig. 15.22 Proposed architectures **a** Downlink fronthaul. **b** Uplink fronthaul

interfering signal is measured at the same location. Figure 15.24 shows the SSR for the 2.5 and 5 GHz SOI.

Maximum SSR of 33 and 43 dB is achieved in the downlink and uplink, respectively, over 8 km SSMF fronthaul distance. The 10 dB SSR gain for the uplink is attributed to the fact that physical-layer signal cancellation physically occurs in stable passive optical components, while in the downlink, it occurs in the wireless multi-path channel, resulting in additional undesired interference. Downlink SSR results in Fig. 15.23 are achieved for intended user versus eavesdropper separations from 0.1 to 0.5 m, confirming efficacy for small-cell scenarios, with similar results also measured for signals at 5 GHz, verifying performance for various frequency bands of prominent wireless standards.

The SSR curves of Figs. 15.23 and 15.24 feature a flat plateau in the 0–10 dBm optical power range, followed by a linear decrease versus optical power governed by PD sensitivity. At SSR = 10 dB, power budgets of 28 and 30 dB are supported by the downlink and uplink, respectively. Finally, from the experiments it may be observed that there is no SSR penalty for increasing fronthaul distance compared to optical back-to-back results. Consequently, so long as minimum PD sensitivity requirements are met, increasing fronthaul reach will only result in optical FIR

coefficient scaling that is proportional to aggregate received power, without degrading SSR integrity.

To assess the bit error rate (BER) of the fronthaul link, downlink and uplink experiments are repeated with a baseband 6 Gbit/s non-return-to-zero (NRZ) pseudorandom binary sequence (PRBS) signal as the SOI. Results for the downlink and uplink architectures shown in Fig. 15.25, reveal a maximum transmission distance of 8 and 18 km SSMF for the downlink and uplink, respectively. The longer uplink transmission distance is attributed to the higher sensitivity of a multimode PD compared to a single mode PD, confirming that both SSR and BER performance are primarily governed by received optical power.

In summary, this investigation experimentally verifies adaptive photonic beamforming for advanced physical-layer security in optical fronthaul of mobile traffic. Up to 33 and 43 dB signal cancellation to undesired eavesdroppers are experimentally demonstrated over 8 km SSMF, with 28 and 30 dB power budgets achieved in downlink and uplink transmission scenarios, respectively. No power penalty is observed by our system. By enhancing physical-layer security with modulation format transparency, the proposed approach is promising for secure optical fronthaul of emerging mobile services.

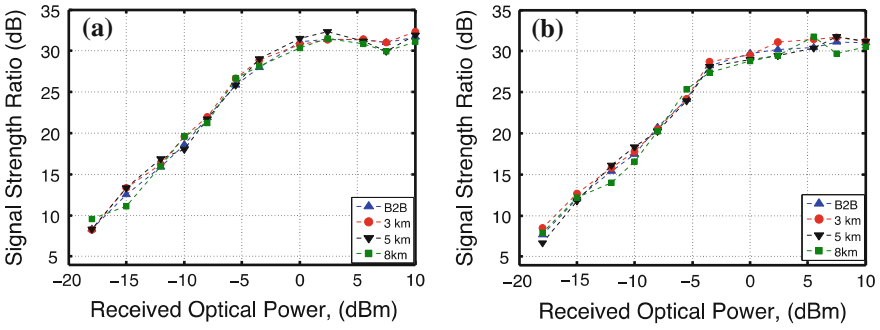

Fig. 15.23 Downlink signal strength ratio. **a** 2.5 GHz SOI. **b** 5 GHz SOI

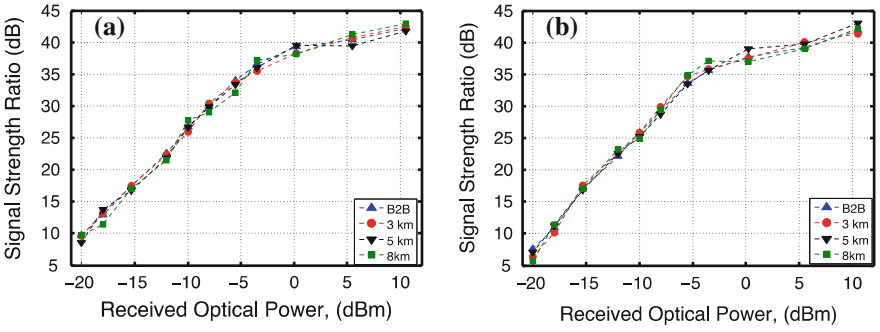

Fig. 15.24 Uplink signal strength ratio. **a** 2.5 GHz SOI. **b** 5 GHz SOI

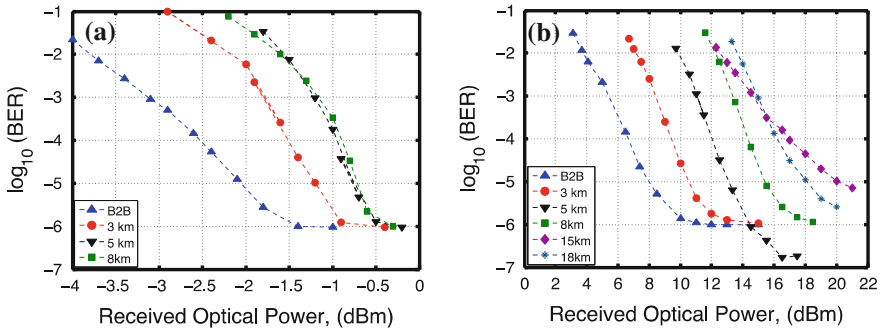

Fig. 15.25 BER versus optical signal power as a function of fronthaul distance. **a** Downlink architecture. **b** Uplink architecture

15.5 Summary and Concluding Remarks

In the past half-decade, wireless communication for data services has witnessed an exponential growth, with the advent of smart phones, WIFI, and wireless bluetooth devices. Mobile apps and computing power has spurred the use of iPhones and Android-powered devices, and it seems a wireless device occupies every pocket. People crave the ability to access anything anywhere at anytime, but, unfortunately, this popularity has caused both significant network burdens and a wireless spectrum crunch. As the growth of mobile Internet traffic continues, the need for an easily implementable method for processing all of this data is essential. Efficient use of the wireless spectrum also creates its own unique requirements.

The growth of wireless bandwidth mirrors the proliferation of optical network bandwidth a decade before, and the backhaul of nearly all wireless data networks is fiber-optic. Analog optical signal processing techniques, or microwave photonics, provides an ideal platform for processing wireless information before it is transported to data aggregation centers by fibers. Photonics offer the advantages not only of broadband operation, but reduced SWAP, in addition to low transmission loss, rapid reconfigurability, and immunity to electromagnetic interference. It is in this context that we presented recent advances in optical signal processing techniques for wireless RF signals. This chapter was devoted to the discussion of photonic architectures for wideband analog signal processing, including RF beamforming and physical layer security.

Beamforming is a technique that utilizes an array of antennas as a spatial and frequency filter to manipulate the beampattern for cancelling unwanted signals. The beamformer uses optical FIR filters to process the signals temporally with thermo-optic optical attenuators to adaptively and rapidly adjust the beampattern. Meanwhile, the geometric configuration of the antennas allows the signals to be processed spatially. Compared to conventional RF beamformers which have limited narrowband performance due to their reliance on electrical phase shifters, the wideband nature of optics offers a clear advantage. The architecture also offers the

distinct advantage of scalability to hundreds of antennas, as needed for practical systems. Such an integrated system could potentially form a frontend of an emerging all-optical signal processing techniques such as photonic neuromorphic processing allowing massive network integration [67–76].

Interference cancellation plays a crucial part in increasing capacity as it enables full duplexing. The ability to reject interference, while receiving an SOI at the same frequency, is referred to as co-channel interference cancellation. Further, a system needs to be adaptive to react to a highly non-stationary environment. Photonic implementations of interference cancellation systems exhibit significant capabilities beyond what is possible with electronic processing.

An emergence of markets relating to mobile applications, such as mobile banking, mobile-to-desktop, and mobile-to-cell towers, will require a high degree of security. Data should only be received by their intended users, and eavesdroppers should not have access to this data. The ultimate form of security is in the physical layer, and it is easiest to place a null in the direction of an eavesdropper. Unlike the software layer, such as encryption or steganography, which can be cracked, physical layer security prevents eavesdroppers from even detecting the presence of data transmission in the first place. This creates a unique application of photonic beamformers for physical layer security in optical fronthaul of mobile traffic.

In summary, this chapter discussed the basic theory of beamforming and the unique challenges of broadband interference cancellation. Next, we presented the requirements and challenges for building optical FIR filters, and reviewed several innovative MPF designs including optical tunable delays and weighting schemes. We also reviewed the state of the art optical beamformers recently proposed and experimentally demonstrated in literature. Furthermore, we detailed a highly scalable photonic beamforming architecture designed for a particularly non-stationary, interfering environment. Finally, we introduced a specific application for the photonic beamformer namely, physical layer security in optical backhaul networks.

We hope that this chapter will contribute to stimulating research in the cross-disciplinary areas of photonics and optics, microwave engineering, wireless communications, and signal processing, from fundamental principles to practical applications.

References

1. Mobile broadband explosion, White Paper, Rysavy Research/4G Americas, Aug 2012
2. H. Bauer, F. Grawert, S. Schink. Semiconductors for wireless communications: growth engine of the industry, McKinsey & Company on Semiconductors, Technical Report (2012)
3. R.A. Monzingo, R.L. Haupt, T.W. Miller, *Introduction to Adaptive Antennas* (SciTech Publishing, Raleigh, 2011)
4. J. Yao, Microwave photonics. J. Lightwave Technol. **27**(3), 314–335 (2009)
5. J. Capmany, B. Ortega, D. Pastor, A tutorial on microwave photonic filters. J. Lightwave Technol. **24**(1), 201–229 (2006)

6. J. Chang, M.P. Fok, J. Meister, P.R. Prucnal, A single source microwave photonic filter using a novel single-mode fiber to multimode fiber coupling technique. Opt. Express **21**(5), 5585–5593 (2013)
7. J. Chang, Y. Deng, M.P. Fok, J. Meister, P.R. Prucnal, A photonic microwave FIR filter using a spectrally sliced supercontinuum source. Appl. Opt. **51**(19), 4265–4268 (2012)
8. J. Chang, P.R. Prucnal, A novel analog photonic method for broadband multipath interference cancellation. IEEE Microwave Wirel. Compon. Lett. **23**(7), 377–379 (2013)
9. R. Haupt, *Antenna Arrays: A Computational Approach* (Wiley, Hoboken, 2010)
10. B. Widrow, P.E. Mantey, L.J. Griffiths, B.B. Goode, Adaptive antenna systems. Proc. IEEE **55**, 2143–2159 (1967)
11. B. Widrow, S.D. Stearns, *Adaptive Signal Processing* (Prentice-Hall, Englewood Cliffs, 1985)
12. L.V. Blake, M.W. Long, *Antennas: Fundamentals, Design, Measurement* (SciTech Publishing, Daryaganj, 2009)
13. S.O. Haykin, *Adaptive Filter Theory* (Prentice-Hall, Englewood Cliffs, 2002)
14. D.B. Hunter, R.A. Minasian, Microwave optical filters using in-fiber Bragg grating arrays. IEEE Microwave Guided Waveguide Lett. **6**(2), 103–105 (1996)
15. X. Yi, R.A. Minasian, New spectrum-sliced microwave photonic filter for high- frequency signal processing. IEEE Photonics Technol. Lett. **21**(4), 230–232 (2009)
16. T. Chen, X. Yi, T. Huang, R.A. Minasian, Spectrum sliced microwave photonic signal processor with tunablity and reconfigurablity, in *Proceeding of the OptoElectronics and Communications Conference* (*OECC*), pp. 1–2, July 2009
17. J. Capmany, J. Mora, D. Pastor, B. Ortega, High-quality online-reconfigurable microwave photonic transversal filter with positive and negative coefficients. IEEE Photonic Technol. Lett. **17**(12), 2730–2732 (2005)
18. X. Yi, T.X.H. Huang, R.A. Minasian, Microwave photonic filter with tunability, reconfigurability and bipolar taps. Electron. Lett. **45**(16), 840–841 (2009)
19. M.D. Manzanedo, J. Mora, J. Capmany, Continuously tunable microwave photonic filter with negative coefficients using cross-phase modulation in an SOA-MZ interferometer. IEEE Photonics Technol. Lett. **20**(7), 526–528 (2008)
20. E.H.W. Chan, R.A. Minasian, Coherence-free equivalent negative tap microwave photonic notch filter based on delayed self-wavelength conversion. IEEE Trans. Microw. Theory Tech. **5**(11), 3199–3205 (2010)
21. J. Mora, A. Martinez, M.D. Manzanedo, J. Capmany, B. Ortega, D. Pastor, Microwave photonic filters with arbitrary positive and negative coefficients using multiple phase inversion in SOA based XGM wavelength converter. Electron. Lett. **41**(16), 53–54 (2005)
22. X. Yi, R.A. Minasian, Novel multitap, flat-top microwave photonic filter based on sinusoidal group delay gratings. J. Lightwave Technol. **26**(15), 2578–2583 (2008)
23. C.-K. Oh, T.-Y. Kim, C.-S. Park, Reconfigurable photonic microwave band-pass filter with negative coefficients based on polarisation modulation. Electron. Lett. **43**(11), 639–641 (2007)
24. S. Mansoori, A. Mitchell, K. Ghorbani, Photonic reconfigurable microwave filter with negative coefficients. Electron. Lett. **40**(9), 541–543 (2004)
25. B. Vidal, J.L. Corral, and J. Marti, Multi-tap all-optical microwave filter with negative coefficients based on multiple optical carriers and dispersive media, in *Proceeding of the International Topical Meeting on Microwave Photonics* (*MWP*), pp. 201–204, Oct 2005
26. D. Pastor, J. Capmany, B. Ortega, A. Martinez, L. Pierno, M. Varasi, Reconfigurable RF photonic filter with negative coefficients and flat-top resonances using phase inversion in a newly designed 2 × 1 integrated Mach-Zehnder modulator. IEEE Photonics Technol. Lett. **16** (9), 2126–2128 (2004)
27. D.B. Hunter, Incoherent bipolar tap microwave photonic filter based on balanced bridge electro-optic modulator. Electron. Lett. **40**(12), 856–858 (2004)
28. L.A. Bui, K.S. Dayaratne, A. Mitchell, Discrete time microwave photonic transversal filter, in *Proceeding of the International Topical Meeting on Microwave Photonics* (*MWP*), pp. 1–3, Oct 2009

29. X. Yi, R.A. Minasian, Dispersion induced RF distortion of spectrum-sliced microwave-photonic filters. IEEE Trans. Microw. Theory Tech. **54**(2), 880–886 (2006)
30. J. Mora, S. Sales, M.D. Manzanedo, R. Garcia-Olcina, J. Capmany, B. Ortega, D. Pastor, Continuous tuning of photonic transversal filter based on the modification of tapped weights. IEEE Photonic Technol. Lett. **18**(15), 1594–1596 (2006)
31. J. Capmany, D. Pastor, B. Ortega, New and flexible fiber-optic delay-line filters using chirped Bragg gratings and laser arrays. IEEE Trans. Microw. Theory Tech. **47**(7), 1321–1326 (1999)
32. W. Liu and S. Weiss. *Wideband Beamforming: Concepts and Techniques* (Wiley, Chichester, 2010)
33. B.D. Van Veen, K.M. Buckley, Beamforming: a versatile approach to spatial filtering. IEEE ASSP Mag. **5**(2), 4–24 (1988)
34. H. Zmuda, R.A. Soref, P. Payson, S. Johns, E.N. Toughlian, Photonic beamformer for phased array antennas using a fiber grating prism, IEEE Photonics Technol. Lett. **9**(2), 241–243 (Feb 1997)
35. M.Y. Frankel, P.J. Matthews, R.D. Esman, Two-dimensional fiber-optic control of a true time-steered array transmitter. IEEE Trans. Microw. Theory Tech. **44**(12), 2696–2702 (1996)
36. L. Yaron, R. Rotman, S. Zach, M. Tur, Photonic beamformer receiver with multiple beam capabilities. IEEE Photonics Technol. Lett. **22**(23), 1723–1725 (2010)
37. L. Jofre, C. Stoltidou, S. Blanch, T. Mengual, B. Vidal, J. Marti, I. Mckenzie, J.M. del Cura, Optically beamformed wideband array performance. IEEE Trans. Antennas Propag. **56**(6), 1594–1604 (2008)
38. H. Subbaraman, M.Y. Chen, R.T. Chen, Simultaneous dual RF beam reception of an X-band phased array antenna utilizing highly dispersive photonic crystal fiber based true-time-delay, in *Proceedings of the Asia Optical Fiber Communication and Optoelectronic Exposition and Conference* (*AOE*), pp 1–3, 2008, paper SaJ2
39. W. Xue, J. Mork, Microwave photonic true time delay based on cross gain modulation in semiconductor optical amplifiers, in *Proceeding of the OptoElectronics and Communications Conference* (*OECC*), pp. 202–203, July 2010
40. M.A. Piqueras, G. Grosskopf, B. Vidal, J. Herrera, J.M. Martinez, P. Sanchis, V. Polo, J.L. Corral, A. Marceaux, J. Galiere, J. Lopez, A. Enard, J.-L. Valard, O. Parillaud, E. Estebe, N. Vodjdani, M.-S. Choi, J.H. den Besten, F.M. Soares, M.K. Smit, J. Marti, Optically beamformed beam-switched adaptive antennas for fixed and mobile broad-band wireless access networks. IEEE Trans. Microw. Theory Tech. **54**(2), 887–899 (2006)
41. Y. Liu, G. Burnham, G. Jin, J. Zhao, Wideband multi-beam photonics-based RF beamformer, in *Proceedings of the IEEE International Symposium on Phased Array Systems and Technology* (*ARRAY*), pp. 581–585, Oct 2010
42. B. Juswardy, F. Xiao, K.E. Alameh, Opto-VLSI-based RF beamformer for space division multiple access network, in *Proceedings of the High-Capacity Optical Networks and Enabling Technologies* (*HONET*), pp. 222–226, Dec 2010
43. H. Zmuda, E. N. Toughlian, Broadband nulling for conformal phased array antennas using photonic processing, in *Proceedings of the International Topical Meeting on Microwave Photonics* (*MWP*), pp. 17–19, Sept 2000
44. D. Marpaung, L. Zhuang, M. Burla, C. Roeloffzen, B. Noharet, Q. Wang, W.P. Beeker, A. Leinse, R. Heideman, Photonic integration and components development for a Ku-band phased array antenna system, in *Proceedings of the International Topical Meeting on Microwave Photonics* (*MWP*), pp. 458–461, Oct 2011
45. L. Zhuang, D. Marpaung, M. Burla, C. Roeloffzen, W. Beeker, A. Leinse, P. van Dijk, Low-loss and programmable integrated photonic beamformer for electronically-steered broadband phased array antennas, in *Proceedings of the IEEE Photonics Conference* (*PHO*), pp. 137–138, 2011
46. J. Chang, M.P. Fok, R.M. Corey, J. Meister, P.R. Prucnal, Highly scalable adaptive photonic beamformer using a single mode to multimode optical combiner. IEEE Microwave Wirel. Compon. Lett. **23**(10), 563–565 (2013)
47. M.P. Fok, Y. Deng, K. Kravtsov, P.R. Prucnal, Signal beating elimination using single-mode fiber to multimode fiber coupling. Opt. Lett. **36**(23), 4578–4580 (2011)

48. S. Lin, K.B. Ng, K.M. Luk, S.S.Wong, A. Poon, A 60 GHz digitally controlled RF beamforming array in 65 nm CMOS with off-chip antennas, in *Proceedings of the Radio Frequency Integrated Circuits Symposium* (*RFIC*), pp. 1–4, June 2011
49. D. Bojic, E. Sasaki, N. Cvijetic, T. Wang, J. Kuno, J. Lessmann, S. Schmid, H. Ishii, S. Nakamura, Advanced wireless and optical technologies for small-cell mobile backhaul with dynamic software-defined management. IEEE Commun. Mag. **51**(9), 86–93 (2013)
50. N. Cvijetic, A. Tanaka, Y.-K. Huang, M. Cvijetic, E. Ip, Y. Shao, T. Wang, 4-G mobile backhaul over OFDMA/TDMA-PON to 200 cell sites per fiber with 10 Gb/s upstream burst-mode operation enabling 1 ms transmission latency, in *Proceedings of the Optical Fiber Communication Conference and Exposition* (*OFC/NFOEC*), 2012, paper PDP5B.7
51. C. Liu, K. Sundaresan, M. Jiang, S. Rangarajan, G.-K. Chang, The case for re-configurable backhaul in cloud-ran based small cell networks, in *Proceedings of the IEEE INFOCOM*, pp. 1124–1132, 2013
52. B.J. Shastri, D.V. Plant, Scaling technologies for terabit fiber optic transmission systems, in *Proceedings of the SPIE*, vol. 7942, (San Francisco, CA, Feb 2011), paper 794206
53. B.J. Shastri, P.R. Prucnal, D.V. Plant, 20-GSample/s (10 GHz × 2 clocks) burst-mode CDR based on injection locking and space sampling for multiaccess networks. IEEE Photonics J. **4** (5), 1783–1793 (2012)
54. B.J. Shastri, D.V. Plant, Truly modular burst-mode CDR with instantaneous phase acquisition for multiaccess networks. IEEE Photonics Technol. Lett. **24**(2), 134–136 (2012)
55. B.J. Shastri, D.V. Plant, 5/10-Gb/s burst-mode clock and data recovery based on semiblind oversampling for PONs: theoretical and experimental. IEEE J. Sel. Top. Quantum Electron. **16** (5), 1298–1320 (2010)
56. B.J. Shastri, Y.B. M'Sallem, N. Zicha, L.A. Rusch, S. LaRochelle, D.V. Plant, Experimental study of burst-mode reception in a 1300 km deployed fiber link. J. Opt. Commun. Networking **2**(1), 1–9 (2010)
57. B.J. Shastri, Z.A. El-Sahn, M. Zeng, N. Kheder, L.A. Rusch, D.V. Plant, A standalone burst-mode receiver with clock and data recovery, clock phase alignment, and RS(255, 239) codes for SAC-OCDMA applications. IEEE Photonics Technol. Lett. **20**(5), 363–365 (2008)
58. Z.A. El-Sahn, B.J. Shastri, M. Zeng, N. Kheder, D.V. Plant, L.A. Rusch, Experimental demonstration of a SAC-OCDMA PON with burst-mode reception: local versus centralized sources. J. Lightwave Technol. **26**(10), 1192–1203 (2008)
59. B. Wu, B.J. Shastri, P.R. Prucnal, Secure communication in fiber-optic networks, in *Emerging Trends in Information and Communication Technologies Security*, ed. by B. Akhgar, H. Arabnia (Elsevier, Waltham, 2013), ch. 11, pp. 173–183
60. B. Wu, Z. Wang, Y. Tian, M.P. Fok, B.J. Shastri, D.R. Kanoff, P.R. Prucnal, Optical steganography based on amplified spontaneous emission noise. Opt. Express **21**(2), 2065–2071 (2013)
61. B. Wu, Z. Wang, B.J. Shastri, M.P. Chang, N.A. Frost, P.R. Prucnal, Temporal phase mask encrypted optical steganography carried by amplified spontaneous emission noise. Opt. Express **22**(1), 954–961 (2014)
62. B. Wu, M.P. Chang, B.J. Shastri, Z. Wang, P.R. Prucnal, Analog noise protected optical encryption with two-dimensional key space. Opt. Express **22**(12), 14568–14574 (2014)
63. B. Wu, B.J. Shastri, P.R. Prucnal, System performance measurement and analysis of optical steganography based on amplifier noise. IEEE Photonics Technol. Lett. **26**(19), 1920–1923 (2014)
64. B. Wu, M.P. Chang, Z. Wang, B.J. Shastri, P.R. Prucnal, Optical encryption based on cancellation of analog noise, in *Proceedings Conference on Lasers and Electro-Optics* (*CLEO*), San Jose, CA, June 2014, paper AW3P.5
65. B. Wu, Z. Wang, B.J. Shastri, Y. Tian, P.R. Prucnal, Phase mask encrypted optical steganography based on amplified spontaneous emission noise, in *Proceedings of the IEEE Photonics Conference* (*IPC*), Seattle, Sept 2013, paper MG3.3, pp. 137–138

66. B. Wu, Z. Wang, B.J. Shastri, Y. Tian, P.R. Prucnal, Two dimensional encrypted optical steganography based on amplified spontaneous emission noise, in *Proceedings of the Conference on Lasers and Electro-Optics* (*CLEO*), San Jose, June 2013, paper AF1H.5
67. A. N. Tait, M.A. Nahmias, Y. Tian, B.J. Shastri, P.R. Prucnal, Photonic neuromorphic signal processing and computing, in *Nanophotonic Information Physics*, ser. Nano-Optics and Nanophotonics, ed. by M. Naruse, Springer, Heidelberg, 2014, pp. 183–222. http://dx.doi.org/10.1007/978-3-642-40224-1_8
68. B.J. Shastri, A.N. Tait, M.A. Nahmias, P.R. Prucnal, Photonic spike processing: ultrafast laser neurons and an integrated photonic network. IEEE Photonics Soc. Newsl. **28**(3), 4–11 (2014)
69. M.A. Nahmias, B.J. Shastri, A.N. Tait, P.R. Prucnal, A leaky integrate-and-fire laser neuron for ultrafast cognitive computing, IEEE J. Sel. Top. Quantum Electron. **19**(5), 1800212 (Sept–Oct 2013)
70. A.N. Tait, M.A. Nahmias, B.J. Shastri, P.R. Prucnal, Broadcast and weight: an integrated network for scalable photonic spike processing. J. Lightwave Technol. **32**(21), 3427–3439 (2014)
71. B.J. Shastri, M.A. Nahmias, A.N. Tait, P.R. Prucnal, Simulations of a graphene excitable laser for spike processing. Opt. Quant. Electron. **46**(10), 1353–1358 (2014)
72. A.N. Tait, B.J. Shastri, M.A. Nahmias, M.P. Fok, P.R. Prucnal, The DREAM: an integrated photonic thresholder. J. Lightwave Technol. **31**(8), 1263–1272 (2013)
73. A.N. Tait, M.A. Nahmias, B.J. Shastri, P.R. Prucnal, Broadcast-and-weight interconnects for integrated distributed processing systems, in *Proceedings of the IEEE Optical Interconnects Conference* (*OI*), Coronado Bay, CA, May 2014, paper WA3, pp. 108–109
74. B.J. Shastri, M.A. Nahmias, A.N. Tait, Y. Tian, B. Wu, P.R. Prucnal, Graphene excitable laser for photonic spike processing, *IEEE Photonics Conf.* (*IPC*), Sept 2013, pp. 1–2. http://dx.doi.org/10.1109/IPCon.2013.6656424
75. M.A. Nahmias, A.N. Tait, B.J. Shastri, P.R. Prucnal, An evanescent hybrid silicon laser neuron, in *Proceedings of the IEEE Photonics Conference* (*IPC*), Seattle, WA, Sept 2013, paper ME3.4, pp. 93–94
76. B.J. Shastri, M.A. Nahmias, A.N. Tait, Y. Tian, M.P. Fok, M.P. Chang, B. Wu, P.R. Prucnal, Exploring excitability in graphene for spike processing networks, in *Proceedings of the IEEE Numerical Simulation of Optoelectronic Devices* (*NUSOD*), Vancouver, Canada, Aug 2013, paper TuC5, pp. 83–84